INTERNATIONAL JOURNAL FOR NUMERICAL METHODS IN ENGINEERING
Int. J. Numer. Meth. Engng 2007; **69**:1262–1277
Published online 31 July 2006 in Wiley InterScience (www.interscience.wiley.com). DOI: 10.1002/nme.1810

Application of hybrid Trefftz finite element method to non-linear problems of minimal surface

Hui Wang[1], Qing-Hua Qin[2,*,†] and Detdexa Arounsavat[2]

[1]*Department of Mechanics, Tianjin University, Tianjin 300072, People's Republic of China*
[2]*Department of Engineering, Australian National University, Canberra, ACT 0200, Australia*

SUMMARY

This investigation provides a hybrid Trefftz finite element approach for analysing minimal surface problems. The approach is based on combining Trefftz finite element formulation with radial basis functions (RBF) and the analogue equation method (AEM). In this method, use of the analogue equation approach avoids the difficulty of treating the non-linear terms appearing in the soap bubble equation, making it possible to solve non-linear problems with the Trefftz method. Global RBF is used to approximate the inhomogeneous term induced from non-linear functions and other loading terms. Finally, some numerical experiments are implemented to verify the efficiency of this method. Copyright © 2006 John Wiley & Sons, Ltd.

Received 20 September 2005; Revised 3 May 2006; Accepted 25 May 2006

KEY WORDS: minimal surface problems; Trefftz finite element method; T-completed solution; the particular solution method; radial basis function; the analogue equation method

1. INTRODUCTION

Soap bubble problems, also known as minimal surfaces problems or Plateau's problems, are defined when the mean curvature is identically zero at any point on a smooth surface [1]. In simple configurations, an analytical solution may be obtained by means of the separate variables method and soap bubble film simulation. However, for some complicated configurations, exact solutions are difficult to obtain due to the high non-linearity of the governing equation. Fortunately, some numerical methods have been developed to analyse such non-linear problems.

*Correspondence to: Qing-Hua Qin, Department of Engineering, Australian National University, Canberra, ACT 0200, Australia.
†E-mail: qinghua.qin@anu.edu.au

Contract/grant sponsor: Australian Research Council; contract/grant number: DP0209487
Contract/grant sponsor: National Natural Science Foundation of China; contract/grant number: 10472082

The first attempt was perhaps that of Douglas [2], who used a finite difference approach to produce a numerical approximation. Tsuchiya [3] gave an existence and convergence proof for discrete minimal surfaces to a continuous solution in the H^1-norm. Lee and Milner [4] proposed a mixed finite element method based on the combination of the h and p version to analyse strongly non-linear second-order elliptic problems and gave numerical implementations for minimal surface problems. Dziuk [5] used the mean curvature flow of surface to compute stable minimal surfaces by finite element method (FEM), and later Dziuk and Hutchinson [6] also presented a general finite element procedure for approximating minimal surfaces, including unstable ones, by means of finding stationary points for the Dirichlet energy within the class of discrete harmonic maps from the discrete unit disc.

As well as domain-type division methods, the boundary element method based on boundary discretization has also been used to obtain approximate solutions of non-linear minimal problems. Wilson [7] proposed a boundary element method using the Douglas integral for the computation of Plateau's problem. Recently, a boundary element solution coupled with the analogue equation method was proposed to solve soap bubble problems [8].

In this paper, a review of the statement of soap bubble problems is given in Section 2. Then in Section 3 a detailed hybrid Trefftz finite element treatment is derived for solving soap bubble problems. Based on the analogue equation method (AEM) [9], the effective combination of Trefftz finite element formulations of Laplacian problems [10] with radial basis functions (RBF) approximation significantly simplifies the complicated variation procedure of standard FEM and, more importantly, all integrals are computed along the boundary of elements only, instead of being domain integral, thereby avoiding direct estimation of fictitious body force terms. Finally, three numerical examples are considered to demonstrate the convergence and stability of the proposed method.

2. STATEMENT OF SOAP BUBBLE PROBLEM/MINIMAL SURFACES [1]

The soap bubble problem is to find a twice continuous differentiable function $u(x, y)$ in a region constrained by bounding contours which minimize the surface area functional

$$A = \int_{\Omega} \sqrt{1 + u_{,x}^2 + u_{,y}^2}\, \mathrm{d}\Omega \tag{1}$$

where a comma followed by a subscript represents differentiation.

The differential equation of this surface area problem is obtained using the Euler–Lagrange condition for minimization of the above functional. This yields the following non-linear boundary value problem (BVP) for the determination of minimal surface

$$(1 + u_{,y}^2)u_{,xx} - 2u_{,x}u_{,y}u_{,xy} + (1 + u_{,x}^2)u_{,yy} = 0 \quad \text{in } \Omega \tag{2}$$

subjected to the Dirichlet boundary condition

$$u = \overline{u}(x, y) \quad \text{on } \Gamma \tag{3}$$

where Ω is a strictly two-dimensional convex domain in $\mathbb{R}^2$ and Γ is its boundary. It is sufficient to assume that the solution to Equation (2) is unique if $\overline{u}(x, y)$, satisfying the bounded slope condition, is the restriction to Γ of a function in the Sobolev space for certain conditions [11].

DOI: 10.1002/nme

Equation (2) is of the elliptic type because its discriminant, namely $(1+u_{,x}^2)(1+u_{,y}^2)-u_{,x}^2u_{,y}^2$, is greater than zero.

Note that Equation (2) describes the shape of a uniformly stretched membrane in the absence of transverse loads when it is bounded by one or more non-intersecting skew space contours in structural analysis. When the slopes are sufficiently small, their squares and products can be neglected and Equation (2) can reduce to the classical Laplace equation [8]

$$\nabla^2 u = u_{,xx} + u_{,yy} = 0 \tag{4}$$

which is the linearized equation of the unloaded membrane.

3. SOLUTION PROCEDURE

To make the solution procedure below more popular and general, we consider a two-dimensional generalized non-linear second-order BVP (see Figure 1)

$$\Re(u, u_{,x}, u_{,y}, u_{,xx}, u_{,yy}, u_{,xy}) = g(x, y) \quad \text{in } \Omega \tag{5}$$

with the following boundary conditions:

$$u = \overline{u} \quad \text{on } \Gamma_u \tag{6a}$$

$$q = \frac{\partial u}{\partial n} = \bar{q} \quad \text{on } \Gamma_q \tag{6b}$$

where $\Re()$ denotes the general differential operator defined in a plane domain Ω bounded by the boundary Γ, $g(x, y)$ is a known function in terms of co-ordinates x and y, n is the normal to the boundary and $\overline{u}$ and $\bar{q}$ are specified single-value functions on the boundary.

The solution to the BVP defined by Equations (5) and (6) is, in general, very complicated due to its non-linearity. In this paper, a general Hybrid Trefftz finite element approach with radial basis

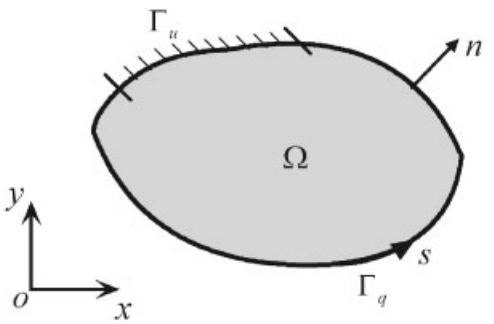

Figure 1. Geometrical definitions and boundary conditions for general non-linear problems.

DOI: 10.1002/nme

function interpolation is developed to solve this category of non-linear problems. The detailed process is presented below.

3.1. The concept of the analogue equation [9]

Suppose that $u = u(x, y)$ is the sought solution to the BVP described by Equations (5) and (6), which is twice continuously differentiable in the domain Ω. If the linear Laplacian operator is applied to this function, that is,

$$\nabla^2 u(x, y) = b(x, y) \quad \text{in } \Omega \tag{7}$$

we can see that Equation (7) implies that a linear equivalent to the non-linear equation (5) is produced. The solutions of Equations (5) and (6) can be established by solving this linear equation (7) under the same boundary conditions (6). Obviously, the fictitious source distribution $b(x, y)$ is related to the unknown function u and an indirect process is described as follows to deal with this obstacle.

3.2. The method of particular solution and radial basis function approximation

Since Equation (7) is linear (if the fictitious source term $b(x, y)$ is viewed as a known function), its corresponding solution can be divided into two parts, a homogeneous solution $u_h(x, y)$ and a particular solution $u_p(x, y)$, that is

$$u = u_h + u_p \tag{8}$$

Accordingly, they should, respectively, satisfy

$$\nabla^2 u_p = b(x, y) \quad \text{in } \Omega \tag{9}$$

and

$$\nabla^2 u_h = 0 \quad \text{in } \Omega \tag{10}$$

with modified boundary conditions

$$u_h = \overline{u}_h = \overline{u} - u_p \quad \text{on } \Gamma_u \tag{11a}$$

$$q_h = \bar{q}_h = \bar{q} - q_p \quad \text{on } \Gamma_q \tag{11b}$$

where $q_h = \partial u_h / \partial n$ and $q_p = \partial u_p / \partial n$.

From above equations we can see that, once the particular solution $u_p(x, y)$ fulfilling Equation (9) is chosen, the homogeneous solution $u_h(x, y)$ is unique.

For the fictitious source distribution $b(x, y)$, we assume [12] that

$$b(x, y) = \sum_{j=1}^{L} \alpha_j f_j(x, y) = \mathbf{f}\boldsymbol{\alpha} \tag{12}$$

DOI: 10.1002/nme

where L is the number of interpolation points, f_j denotes the basis function used for interpolation, and α_j represents the set of interpolating coefficients. Theoretically, any basis function can be used for interpolation. However, radial basis functions have been found to be most suitable for interpolating the fictitious source $b(x, y)$ [13–15]. Radial basis functions usually are expressed in terms of the Euclidian distance, so they can work well in any dimensional space and does not increase the computational difficulty. In most numerical analyses, the commonly used RBFs are:

- linear polynomial: $f_j = 1 + r_j$,
- thin plate spline (TPS): $f_j = r_j^2 \ln r_j$,
- multiquadric (MQ): $f_j = \sqrt{r_j^2 + c^2}$,

where r_j represents the Euclidean distance of the given point (x, y) from a fixed point (x_j, y_j) in the domain of interest.

It is worth pointing out that the linear polynomial and TPS are piecewise smooth in the space, while MQ is infinitely smooth. Due to the sensitivity to shape parameter c, MQ does not be suggested to be used in the paper, although it can reach good accuracy in some cases.

At the same time, it is reasonable to assume

$$u_p(x, y) = \sum_{j=1}^{L} \alpha_j \hat{u}_j = \hat{\mathbf{u}}\boldsymbol{\alpha} \tag{13a}$$

$$q_p(x, y) = \frac{\partial u_p}{\partial n} = \sum_{j=1}^{L} \alpha_j \hat{q}_j = \hat{\mathbf{q}}\boldsymbol{\alpha} \quad \left(\hat{q}_j = \frac{\partial \hat{u}_j}{\partial n}\right) \tag{13b}$$

if a relationship between f_j and $\hat{u}_j$ such as

$$\nabla^2 \hat{u}_j = f_j \tag{14}$$

exists.

Since the fictitious source distribution $b(x, y)$ is determined by the unknown function u, the particular solution and its normal derivative cannot be directly determined using the formulation in this section. However, this formulation still contributes to constructing the approximated expression of the unknown function u.

3.3. Trefftz finite element method

In this section, we apply the theory of Trefftz finite element method [10] to the homogeneous linear BVP consisting of Equations (10) and (11).

For a particular element, say element e, we assume fields:

(a) *The non-conforming intra-element field*:

$$u_{eh}(x, y) = \sum_{j=1}^{m} N_{ej} c_{ej} = \mathbf{N}_e \mathbf{c}_e \tag{15}$$

where $\mathbf{c}_e$ is a vector of undetermined coefficients and m is its number of components. N_{ej} are homogeneous solutions to Equation (10) obtained by a suitably truncated T-complete solution.

DOI: 10.1002/nme

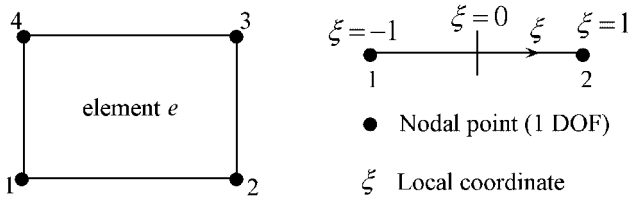

Figure 2. Typical two-dimensional four-node element with linear frame function.

For example,

$$N_{e(2n-1)} = r_e^n \cos n\theta_e, \quad N_{e(2n)} = r_e^n \sin n\theta_e \quad (n = 1, 2, \ldots) \tag{16}$$

for a two-dimensional problem with a bounded domain.

With regard to the proper number m of trial functions N_{ej} for the element, the basic rule used to prevent spurious energy modes is analogous to that in the hybrid-stress model. The necessary (but not sufficient) condition is stated as

$$m \geqslant k - r \tag{17}$$

where k is the number of nodal degree of freedom (DOF) of the element under consideration and r represents the discarded rigid body motion terms. For instance, $r = 1$ in the Poisson equation and $r = 3$ in the 2D linear elastic case.

Additionally, the corresponding outward normal derivative of u_{eh} on Γ_e is

$$q_{eh} = \frac{\partial u_{eh}}{\partial n} = \mathbf{T}_e \mathbf{c}_e \tag{18}$$

where $\mathbf{T}_e = \partial \mathbf{N}_e / \partial n$.

(b) *An auxiliary conforming frame field*: In order to enforce on u_h the conformity, for instance, $u_{eh} = u_{fh}$ on $\Gamma_e \cap \Gamma_f$ of any two neighboring elements, we use an auxiliary inter-element frame field $\tilde{u}_h$ approximated in terms of the same DOF, $\mathbf{d}$, as used with the conventional elements. In this case, as standard HT element, $\tilde{u}_h$ is confined to the whole element boundary, that is,

$$\tilde{u}_{eh}(x, y) = \tilde{\mathbf{N}}_e \mathbf{d}_e \tag{19}$$

which is independently assumed along the element boundary in terms of nodal DOF $\mathbf{d}_e$, where $\tilde{\mathbf{N}}_e$ represents the conventional finite element interpolating functions. For example, a simple interpolation of the frame field on the side 2–3 of a particular element (Figure 2) can be given in the form

$$\tilde{u}_{23} = \tilde{N}_1 u_2 + \tilde{N}_2 u_3 \tag{20}$$

where

$$\tilde{N}_1 = \frac{1 - \xi}{2}, \quad \tilde{N}_2 = \frac{1 + \xi}{2} \tag{21}$$

DOI: 10.1002/nme

(c) *Jirousek's variational principle* [*10, 16*]: The variational functional Π corresponding to the whole system can be written as the sum of E element quantities Π_e as

$$\Pi = \sum_{e=1}^{E} \Pi_e \tag{22}$$

where E is the total number of elements, and Π_e is the variational functional related to a particular element e, which is expressed as [10]

$$\Pi_e = -\frac{1}{2}\int_{\Omega_e} (q_1^2 + q_2^2)\,\mathrm{d}\Omega - \int_{\Gamma_{eu}} q_h \overline{u}_h\,\mathrm{d}\Gamma + \int_{\Gamma_{eq}} (\bar{q}_h - q_h)\tilde{u}_h\,\mathrm{d}\Gamma - \int_{\Gamma_{eI}} q_h \tilde{u}_h\,\mathrm{d}\Gamma \tag{23}$$

where Ω_e stands for the eth element sub-domain, $\Gamma_e = \Gamma_{eu} + \Gamma_{eq} + \Gamma_{eI}$, while $\Gamma_{eu} = \Gamma_e \cap \Gamma_u$, $\Gamma_{eq} = \Gamma_e \cap \Gamma_q$, and Γ_{eI} is the inter-element boundary of element e.

Integrating the domain integral term in Equation (23) by parts, we obtain

$$\Pi_e = \frac{1}{2}\int_{\Gamma_e} q_h u_h\,\mathrm{d}\Gamma - \int_{\Gamma_{eu}} q_h \overline{u}_h\,\mathrm{d}\Gamma + \int_{\Gamma_{eq}} (\bar{q}_h - q_h)\tilde{u}_h\,\mathrm{d}\Gamma - \int_{\Gamma_{eI}} q_h \tilde{u}_h\,\mathrm{d}\Gamma \tag{24}$$

Substituting Equations (15), (18) and (19) into the functional (24) produces

$$\Pi_e = -\tfrac{1}{2}\mathbf{c}_e{}^{\mathrm{T}}\mathbf{H}_e\mathbf{c}_e + \mathbf{c}_e{}^{\mathrm{T}}\mathbf{S}_e\mathbf{d}_e + \mathbf{c}_e{}^{\mathrm{T}}\mathbf{r}_{1e} + \mathbf{d}_e{}^{\mathrm{T}}\mathbf{r}_{2e} \tag{25}$$

where

$$\mathbf{H}_e = -\int_{\Gamma_e} \mathbf{T}_e{}^{\mathrm{T}}\mathbf{N}_e\,\mathrm{d}\Gamma$$

$$\mathbf{S}_e = -\int_{\Gamma_{eq}\cup\Gamma_{eI}} \mathbf{T}_e{}^{\mathrm{T}}\tilde{\mathbf{N}}_e\mathrm{d}\Gamma$$

$$\mathbf{r}_{1e} = -\int_{\Gamma_{eu}} \mathbf{T}_e{}^{\mathrm{T}}\overline{u}_h\,\mathrm{d}\Gamma = -\int_{\Gamma_{eu}} \mathbf{T}_e^{\mathrm{T}}(\overline{u} - \hat{\mathbf{u}}\boldsymbol{\alpha})\mathrm{d}\Gamma$$

$$= -\int_{\Gamma_{eu}} \mathbf{T}^{\mathrm{T}}\overline{u}\,\mathrm{d}\Gamma + \left(\int_{\Gamma_{eu}} \mathbf{T}_e{}^{\mathrm{T}}\hat{\mathbf{u}}\,\mathrm{d}\Gamma\right)\boldsymbol{\alpha} = \mathbf{r}_{1e}(\boldsymbol{\alpha})$$

$$\mathbf{r}_{2e} = \int_{\Gamma_{eq}} \tilde{\mathbf{N}}_e{}^{\mathrm{T}}\bar{q}_h\,\mathrm{d}\Gamma = \int_{\Gamma_{eq}} \tilde{\mathbf{N}}_e{}^{\mathrm{T}}(\bar{q} - \hat{\mathbf{q}}\boldsymbol{\alpha})\mathrm{d}\Gamma$$

$$= \int_{\Gamma_{eq}} \tilde{\mathbf{N}}_e{}^{\mathrm{T}}\bar{q}\,\mathrm{d}\Gamma - \left(\int_{\Gamma_{eq}} \tilde{\mathbf{N}}_e{}^{\mathrm{T}}\hat{\mathbf{q}}\,\mathrm{d}\Gamma\right)\boldsymbol{\alpha} = \mathbf{r}_{2e}(\boldsymbol{\alpha})$$

DOI: 10.1002/nme

For the minimization of the functional Π, using the necessary conditions:

$$\frac{\partial \Pi}{\partial \mathbf{c}^{\mathrm{T}}} = \sum_{e=1}^{E} \frac{\partial \Pi_e}{\partial \mathbf{c}^{\mathrm{T}}} = \sum_{e=1}^{E} \frac{\partial \Pi_e}{\partial \mathbf{c}_e^{\mathrm{T}}} = \mathbf{0} \tag{26}$$

$$\frac{\partial \Pi}{\partial \mathbf{d}^{\mathrm{T}}} = \sum_{e=1}^{E} \frac{\partial \Pi_e}{\partial \mathbf{d}^{\mathrm{T}}} = \sum_{e=1}^{E} \frac{\partial \Pi_e}{\partial \mathbf{d}_e^{\mathrm{T}}} = \mathbf{0} \tag{27}$$

we can obtain

$$-\mathbf{Hc} + \mathbf{Sd} + \mathbf{r}_1 = \mathbf{0} \tag{28}$$

$$\mathbf{S}^{\mathrm{T}}\mathbf{c} + \mathbf{r}_2 = \mathbf{0} \tag{29}$$

where $\mathbf{c}$ and $\mathbf{d}$ are the total coefficients vector of T-complete functions interpolation and nodal unknowns related to the full system, respectively. $\mathbf{H} = \sum_{e=1}^{E} \mathbf{H}_e$, $\mathbf{S} = \sum_{e=1}^{E} \mathbf{S}_e$, $\mathbf{r}_1 = \sum_{e=1}^{E} \mathbf{r}_{1e}$ and $\mathbf{r}_2 = \sum_{e=1}^{E} \mathbf{r}_{2e}$.

Equations (27) and (28) lead to

$$\mathbf{c} = \mathbf{Gd} + \mathbf{g} \tag{30a}$$

$$\mathbf{Kd} = \mathbf{p}(\boldsymbol{\alpha}) \tag{30b}$$

where $\mathbf{G} = \mathbf{H}^{-1}\mathbf{S}$, $\mathbf{g} = \mathbf{H}^{-1}\mathbf{r}_1$, $\mathbf{K} = \mathbf{G}^{\mathbf{T}}\mathbf{HG}$ and $\mathbf{p} = -\mathbf{G}^{\mathbf{T}}\mathbf{Hg} - \mathbf{r}_2$.

Consequently, vectors $\mathbf{c}$ and $\mathbf{d}$ are expressed in terms of the unknown interpolation coefficient $\boldsymbol{\alpha}$ by means of Equations (30a) and (30b).

(d) *Finding the discarded rigid body motion terms*: It suffices to reintroduce the discarded modes in the internal field u_{eh} of a particular element and then to calculate their undetermined coefficients by requiring, for example, the least squares adjustment of u_{eh} and $\tilde{u}_{eh}$. In this case, these missing terms can easily be recovered by setting for the augmented internal field

$$u_{eh}(x, y) = \mathbf{N}_e\mathbf{c}_e + c_0 \tag{31}$$

and using a least-square procedure to match u_{eh} and $\tilde{u}_{eh}$ at nodes of the element boundary Γ_e:

$$\sum_{i=1}^{N_e} (u_{eh} - \tilde{u}_{eh})^2|_{\text{node } i} = \min \tag{32}$$

where N_e is the number of nodes for the element under consideration. The above equation finally yields

$$\sum_{i=1}^{N_e} (N_e c_e + c_0 - \tilde{u}_{eh})|_{\text{node } i} = 0 \tag{33}$$

Then, we have

$$c_0 = \frac{1}{N_e} \sum_{i=1}^{N_e} (\tilde{u}_{eh} - \mathbf{N}_e\mathbf{c}_e)|_{\text{node } i} \tag{34}$$

DOI: 10.1002/nme

3.4. Final non-linear equations

At an arbitrary point (x, y) in element e, the full solution can be expressed as

$$u(x, y) = u_h|_{(x,y)} + u_p|_{(x,y)} = \hat{\mathbf{u}}|_{(x,y)}\boldsymbol{\alpha} + \mathbf{N}|_{(x,y)}\mathbf{c} + c_0 = \mathbf{u}(\boldsymbol{\alpha}) \tag{35}$$

Furthermore, the related derivatives can also be obtained

$$u_{,x}(x, y) = \hat{\mathbf{u}}_{,x}|_{(x,y)}\boldsymbol{\alpha} + \mathbf{N}_{,x}|_{(x,y)}\mathbf{c} = \mathbf{u}_{,x}(\boldsymbol{\alpha}) \tag{36a}$$

$$u_{,y}(x, y) = \hat{\mathbf{u}}_{,y}|_{(x,y)}\boldsymbol{\alpha} + \mathbf{N}_{,y}|_{(x,y)}\mathbf{c} = \mathbf{u}_{,y}(\boldsymbol{\alpha}) \tag{36b}$$

$$u_{,xx}(x, y) = \hat{\mathbf{u}}_{,xx}|_{(x,y)}\boldsymbol{\alpha} + \mathbf{N}_{,xx}|_{(x,y)}\mathbf{c} = \mathbf{u}_{,xx}(\boldsymbol{\alpha}) \tag{36c}$$

$$u_{,xy}(x, y) = \hat{\mathbf{u}}_{,xy}|_{(x,y)}\boldsymbol{\alpha} + \mathbf{N}_{,xy}|_{(x,y)}\mathbf{c} = \mathbf{u}_{,xy}(\boldsymbol{\alpha}) \tag{36d}$$

$$u_{,yy}(x, y) = \hat{\mathbf{u}}_{,yy}|_{(x,y)}\boldsymbol{\alpha} + \mathbf{N}_{,yy}|_{(x,y)}\mathbf{c} = \mathbf{u}_{,yy}(\boldsymbol{\alpha}) \tag{36e}$$

In order to determine the unknown coefficient $\boldsymbol{\alpha}$, it should be forced to satisfy the governing Eqaution (2) at L interpolating points, that is

$$\Re(\boldsymbol{\alpha})|_{(x_i,y_i)} = g(x_i, y_i) \quad (x_i, y_i) \in \Omega, \quad i = 1, 2, \ldots, L \tag{37}$$

from which the unknown coefficients vector $\boldsymbol{\alpha}$ can be determined by means of iterative algorithms. In this paper, the Newton–Raphson iteration method appearing in Reference [17] is employed to solve the non-linear equation (37).

It is clear that once all unknowns are determined, the distribution of field u at any point in the domain can be calculated using Equation (35).

4. NUMERICAL IMPLEMENTATION

To demonstrate the proposed numerical model, two numerical examples are considered in this section. In the process of computation, the classic RBF $f = 1 + r$ [14] is employed and it is convenient to choose nodal points and the central points of elements as the interpolation points to simplify preparation of input data. At the same time, the standard four-node quadrangular element is used to perform the calculation. Consequently, the minimal number of terms m of T-complete trial functions satisfying the necessary condition (17) is easily determined ($m \geqslant 4 - 1 = 3$). It should be mentioned that, in the calculation, a zero initial guess as to the unknown interpolating coefficients is assumed unless otherwise stated. In addition, the nodes and the central points of elements are chosen as the interpolation points in the process of computation.

Due to the complication of minimal surface problems, the analytical solution is difficult to be obtained. In the paper, in order to demonstrate the accuracy of proposed method, results obtained by Matlab PDE toolbox are employed to provide rough comparison. Matlab PDE toolbox is designed to

DOI: 10.1002/nme

solve the linear and non-linear filed equations, for instance, Poisson equation, Helmholtz equation, and so on, by means of finite element method with triangle element.

4.1. Example 1. A square domain with unit side length

As a first example, we consider the minimal surface problems in a unit square. The boundary conditions are

$$\overline{u}(x, y) = \begin{cases} \ln \dfrac{\cos(y - 0.5)}{\cos(-0.5)}, & 0 \leqslant y \leqslant 1, \quad x = 0 \\ \ln \dfrac{\cos(y - 0.5)}{\cos(0.5)}, & 0 \leqslant y \leqslant 1, \quad x = 1 \\ \ln \dfrac{\cos(0.5)}{\cos(x - 0.5)}, & 0 \leqslant x \leqslant 1, \quad y = 1 \\ \ln \dfrac{\cos(-0.5)}{\cos(x - 0.5)}, & 0 \leqslant x \leqslant 1, \quad y = 0 \end{cases} \tag{38}$$

so that the exact solution has an expression such as

$$u(x, y) = \ln \frac{\cos(y - 0.5)}{\cos(x - 0.5)} \tag{39}$$

which can be used to scale our numerical results.

In our analysis, the average relative error defined by

$$\text{Arerr}(u) = \sqrt{\frac{\sum_{j=1}^{M} (u_j - \tilde{u}_j)^2}{\sum_{j=1}^{M} (u_j)^2}} \tag{40}$$

is used to study convenient performance, where u_j and $\tilde{u}_j$ are respectively the analytical and numerical results at the points considered and M is the total number of these points.

In the numerical analysis, four different meshes (2×2, 5×5, 8×8 and 10×10) are used to model the square domain in order to assess the convergent performance of the proposed method. 441 points in total are selected to evaluate the Arerr(u). Figure 3 shows the variation of the average relative error with the mesh density. It is evident from Figure 3 that the results show a good convergent performance along with refinement of the element mesh. The numbers of iterations corresponding to the four meshes are 1, 11, 8 and 7, respectively. Because the Newton–Raphson iteration employed includes the line search process [17], which is used to obtain a descent direction, there are many potential search substeps at each iteration.

The results of the effect of the number of T-complete trial functions are shown in Figure 4. It is evident that the increase in m does not present obvious improvement in numerical results, but does

DOI: 10.1002/nme

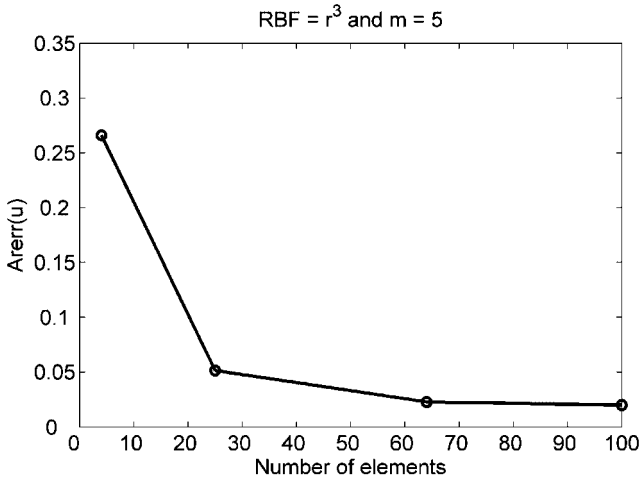

Figure 3. Variation of the average relative error as the meshes refine with $m = 5$ (x, y, x^2, y^2, xy).

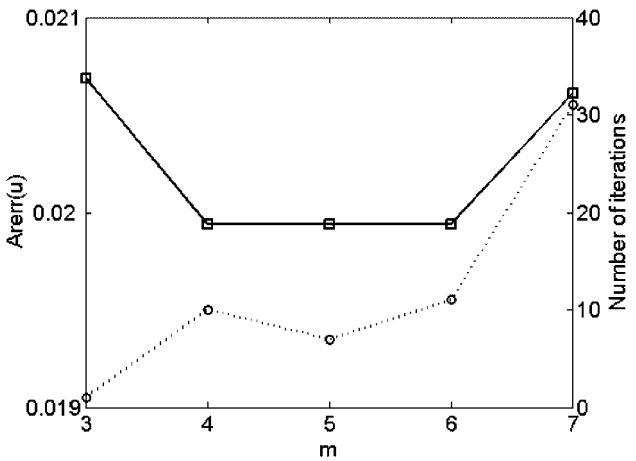

Figure 4. Effect of the number of terms m of T-complete trail functions when 10×10 meshes are employed.

require increased computational quantity. Therefore the conclusion can be drawn that the proposed method is not sensitive to number m when $m \geqslant 3$.

Finally, the distribution of absolute error in u and the comparison of the minimal surface and its isoline between the exact solution and numerical results are plotted in Figures 5 and 6 , respectively. As expected, the results obtained from the proposed formulation show a good agreement with

DOI: 10.1002/nme

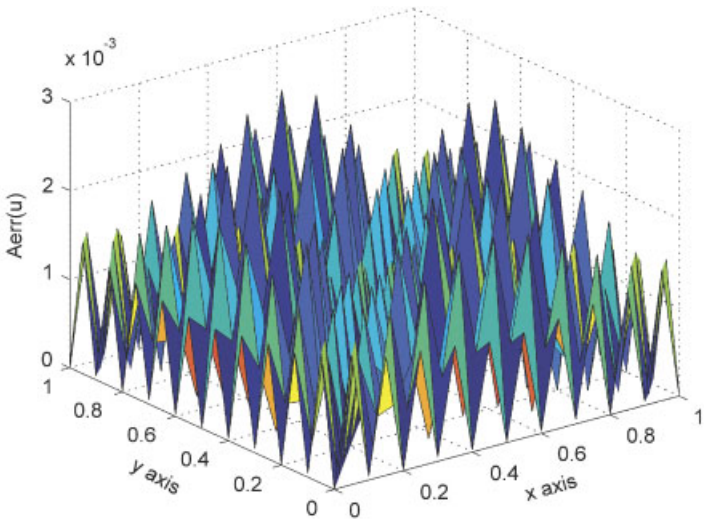

Figure 5. Absolute error distribution in u at the 441 test points uniformly distributed in the domain when 10×10 meshes are employed and $m = 5$.

analytical results. It is also found from the two figures that the results show fully symmetry about the lines $x = 0.5$ and $y = 0.5$ and anti-symmetry about the line $x = y$ and $-y$.

4.2. Example 2. Square membrane with side length 1

In this case, we again take into account a square membrane with boundary conditions as shown in Figure 7, from which we can see that the boundary conditions are anti-symmetric with respect to the diagonal $x = y$.

In computation, the square domain is discretized using 10×10 meshes and the number of terms of T-complete functions is taken to be 5. Converged results were achieved after 4 iterations. In Table I, the comparison between the Matlab PDE toolbox and the present method is shown and the similar results are observed. The corresponding minimal surface and isoline map are shown in Figure 8. It is evident from Figure 8 that the antisymmetric feature about the diagonal $x = y$ is fully revealed and the values on the boundary exhibit good accuracy in comparison with analytical values. For example, numerical results at the boundary points (0.55, 0) and (1, 0.55), which are not at nodes, are 0.3049, 0.6950, respectively, and the related analytical values are 0.3025 and 0.6975.

4.3. Example 3. Two parallel rings with aligned centres

As the third example, we consider the ring domain shown in Figure 9. The inner and outer radii are 0.5 and 1, respectively, and the related boundary conditions are 0.5 and 1, respectively.

In our computation, 72 four-node quadrilateral elements are used to discretize the entire ring and five terms of T-complete functions are employed. In this example, we compare the results obtained by means of Matlab PDE toolbox and the Hybrid Trefftz method, respectively, in Table II, from

DOI: 10.1002/nme

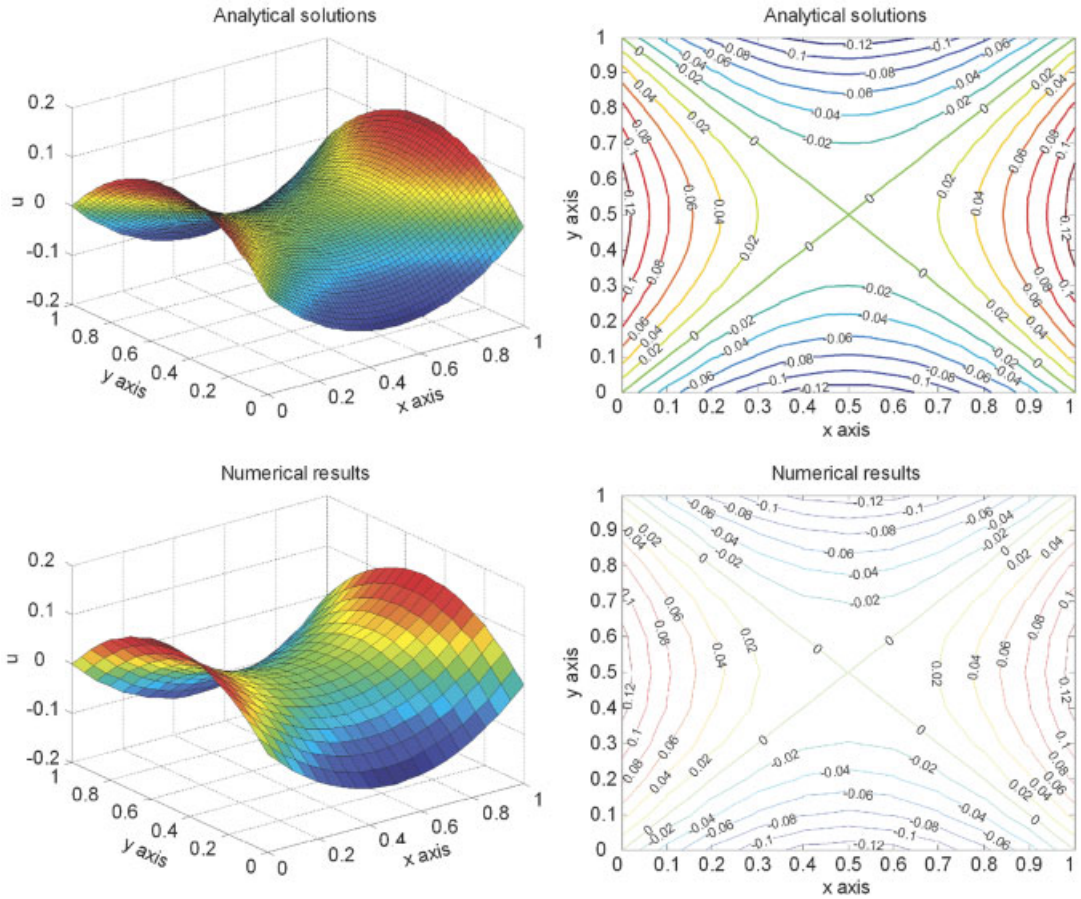

Figure 6. The analytical and approximated minimal surfaces and isolines in the square domain when 10×10 meshes are employed and $m = 5$.

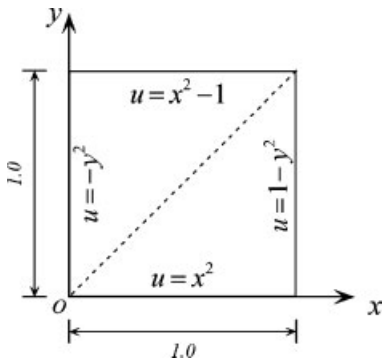

Figure 7. Geometry of the square domain and boundary conditions.

DOI: 10.1002/nme

Table I. Comparison between the Matlab PDE toolbox and the presented method.

x	y	Matlab PDE toolbox	Trefftz FEM
0.9564	0.0480	0.9071	0.9123
0.5579	0.2370	0.2248	0.2552
0.7456	0.8416	−0.1391	−0.1522
0.0439	0.9519	−0.9002	−0.9042
0.9114	0.8441	0.1125	0.1166
0.6299	0.6545	−0.0280	−0.0320
0.5148	0.8310	−0.3834	−0.4264
0.8242	0.5850	0.3044	0.3377

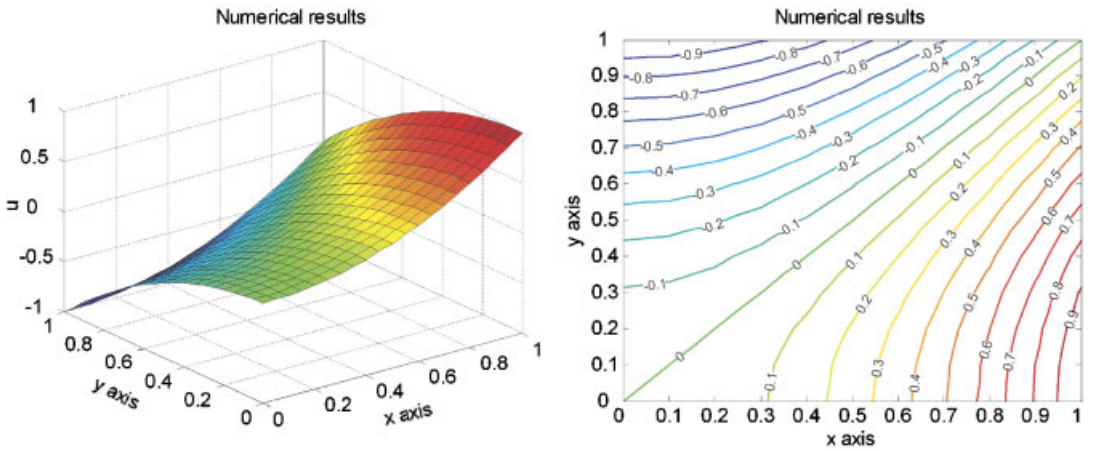

Figure 8. The approximated minimal surface and isoline distribution in the square domain when 10×10 meshes are employed and $m = 5$.

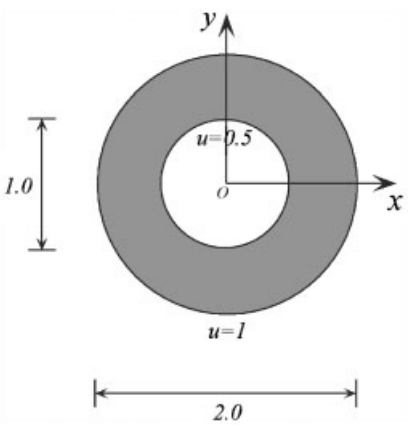

Figure 9. Hollow ring domain and the related boundary conditions.

DOI: 10.1002/nme

Table II. Comparison between the Matlab PDE toolbox and the presented method.

x	y	Matlab PDE toolbox	Trefftz FEM
1.0000	0.0000	1.0000	1.0027
0.8708	0.1269	0.9276	0.9079
0.8139	0.2595	0.9111	0.8866
0.5562	0.6212	0.8968	0.8702
0.5992	0.4457	0.8270	0.7882
0.6374	0.2704	0.7818	0.7350
0.5994	0.1151	0.6804	0.6418
0.5000	0.0000	0.5000	0.5000

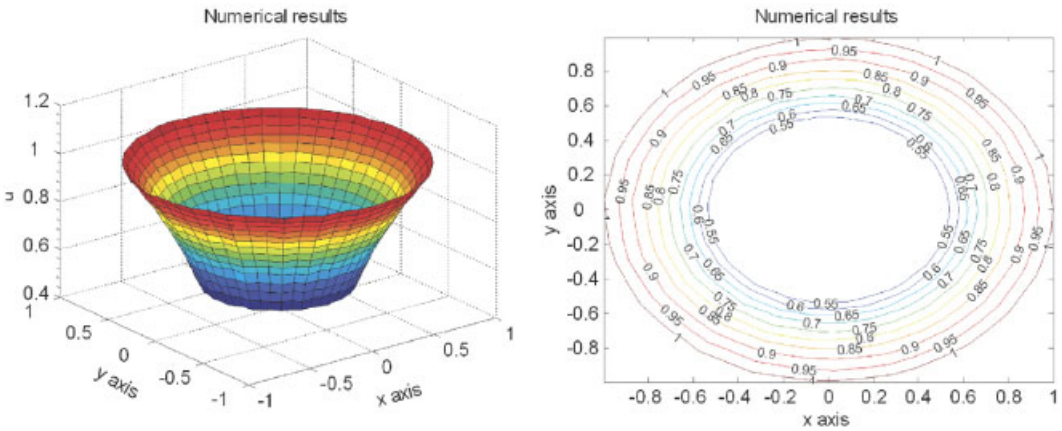

Figure 10. The approximated minimal surface and isoline distribution in the ring when 72 elements are employed and $m = 5$.

which we can see that the former has the similar results as the latter. Consequently, the distribution of the minimal surface and the related isoline map are displayed in Figure 10 by means of the proposed method.

5. CONCLUDING REMARKS

In this paper a hybrid Trefftz finite element method combining radial basis function interpolation and the analogue equation method is developed to solve non-linear soap bubble problems. It is noted that progress in the development of the non-linear Trefftz FEM is quite slow. This is due to the lower computing efficiency in evaluating non-linear terms and body force terms. The introduction of the analogue equation method and radial basis function can avoid the domain integral on these terms and thus make computation more simple and efficient. The proposed method also displays

DOI: 10.1002/nme

the following main features:

- The complex variations of non-linear soap bubble problems are avoided, being replaced by the simple Laplacian variation equation.
- The derivation of Equation (35) is fully independent of the specified soap bubble problems. Thus the proposed method is versatile and can easily extend to other linear and non-linear problems.
- All integrals are performed on the element boundary only.

Finally, it should be noted that the main aim of this paper is to present a new approach for solving non-linear minimal surface problems, instead of developing a successful iteration algorithm. So, for the strong non-linear cases, that is, the larger slope, the standard iterative algorithm maybe is difficult to reach convergence results. In this case, the proper damping strategy, for example, *Armijo–Goldstein line search*, and so on, usually are used to obtain a descent direction.

ACKNOWLEDGEMENTS

This work was financially supported by both Australian Research Council (Grant No. DP0209487) and the National Natural Science Foundation of China (Grant No. 10472082). The support is fully acknowledged.

REFERENCES

1. Struwe M. *Plateau's Problem and the Calculus of Variations*. Princeton University Press: Princeton, NJ, 1988.
2. Douglas J. A method of numerical solution of the plateau problem. *Annals of Mathematics* 1928; **29**:180–188.
3. Tsuchiya T. Discrete solution of the plateau problem and its convergence. *Mathematics of Computation* 1987; **49**:157–165.
4. Lee M, Milner FA. Mixed finite element methods for nonlinear elliptic problems: the *h-p* version. *Journal of Computational and Applied Mathematics* 1997; **85**:239–261.
5. Dziuk G. An algorithm for evolutionary surfaces. *Numerische Mathematik* 1991; **58**:603–611.
6. Dziuk G, Hutchinson JE. The discrete plateau problem: algorithm and numerics. *Mathematics of Computation* 1999; **68**:1–23.
7. Wilson WL. On discrete dirichlet and plateau problem. *Numerische Mathematik* 1961; **3**:359–373.
8. Katsikadelis JT, Nerantzaki MS. A boundary element solution to the soap bubble problem. *Computational Mechanics* 2001; **27**:154–159.
9. Katsikadelis JT. The analog equation method. A powerful BEM-based solution technique for solving linear and nonlinear engineering problems. In *Boundary Element Method XVI*, Brebbia CA (ed.). Computational Mechanics Publications: Southampton.
10. Qin QH. *The Trefftz Finite and Boundary Element Method*. WIT Press: Southampton, Boston, 2000.
11. Morrey CB. *Multiple Integrals in the Calculus of Variations*. Berlin: Springer, 1966.
12. Nardini D, Brebbia CA. A new approach to free vibration analysis using boundary elements. In *Boundary Element Methods in Engineering Proceedings*, Brebbia CA (ed.); *4th International Seminar*, Southampton, Springer-Verlag: Berlin, 1982; 312–326.
13. Golberg MA, Chen CS. *Discrete Projection Methods for Integral Equations*. Computational Mechanics Publications: Southampton, Boston, 1996.
14. Partridge PW, Brebbia CA, Wrobel LC. *The Dual Reciprocity Boundary Element Method*. Computational Mechanics Publications: Southampton, Boston, 1992.
15. Schaback R. Error estimates and condition numbers for radial basis function interpolation. *Advances in Computational Mathematics* 1995; **3**:251–264.
16. Jirousek J, Guex L. The hybrid-Trefftz finite element model and its application to plate bending. *International Journal for Numerical Methods in Engineering* 1986; **23**:651–693.
17. Press WH, Teukolsky SA, Vetterling WT, Flannery BP. *Numerical Recipes in Fortran 77* (2nd edn). Cambridge University Press: Cambridge, MA, 2001.

DOI: 10.1002/nme